Journal of Materials Chemistry A

COMMUNICATION

View Article Online
View Journal | View Issue

Cite this: J. Mater. Chem. A, 2016, 4, 3217

Received 21st December 2015
Accepted 28th January 2016

DOI: 10.1039/c5ta10461k

www.rsc.org/MaterialsA

Elastic and wearable ring-type supercapacitors†

Lie Wang, Qingqing Wu, Zhitao Zhang, Ye Zhang, Jian Pan, Yiming Li, Yang Zhao, Lijuan Zhang,* Xunliang Cheng and Huisheng Peng*

The development of flexible energy storage devices is critical while it remains challenging for wearable electronics. Herein, a new family of elastic and wearable ring-type supercapacitors is fabricated by winding aligned carbon nanotube/poly(3,4-ethyl-enedioxy-thiophene):poly(styrene sulfonate) composite sheets onto an elastic polymer ring. The supercapacitor delivers a high specific capacitance of 134.8 F g^{-1} at a current density of 1 A g^{-1}. Importantly, the specific capacitance has been well maintained after expanding and pressing, which endows the supercapacitor with unique advantages, *e.g.*, it can be used for substrates with different sizes and shapes and may satisfy a variety of wearable applications as well as other fields.

Introduction

Wearable electronic devices have recently attracted increasing attention as an important branch of modern electronics. To this end, it is critically important to develop flexible, lightweight and effective energy storage systems, which are indispensable parts to power wearable devices.[1–4] Supercapacitors are of significant interest in energy storage due to their combined advantages including high power density, short charging time, long cycling life and high safety.[5,6] Unfortunately, conventional supercapacitors appear as a bulky structure and are heavy and rigid, which mismatches the requirements for flexibility in wearable applications.[7,8] Recently, flexible supercapacitors have been also achieved by making them thin,[7,9,10] but the planar configuration has limited their wearable applications in a variety of fields in nature. For instance, they cannot be closely attached onto curved and irregular surfaces of our bodies. Therefore, the development of new configurations is highly required to achieve wearable supercapacitors. To this end, a family of flexible fiber-shaped supercapacitors in one-dimension has been proposed to solve the above problem.[11,12] However, the thin fiber-shaped supercapacitors can offer limited power capabilities, and it also remains challenging to continuously produce them at an application scale and weave them into textiles to power wearable devices as expected.

Besides textiles that are widely recognized as a main wearable format, a broad spectrum of the other wearable products that appear as rings have been also extensively used in our lives, *e.g.*, necklaces, bracelets and finger rings. They can be directly and easily worn on our bodies with unique and promising advantages.[13,14] For instance, they can be worn on the irregular substrates of our bodies, and they also apply to the bodies with different sizes after being made stretchable. Actually, some conceptually new wearable electronic products in a ring configuration, such as Microsoft Band, NFC Ring, and Flyfit, have recently emerged as state-of-the-art technology. If a supercapacitor is made into a ring shape, it can better satisfy these new wearable applications and the other urgent requirements. To the best of our knowledge, such a ring-type supercapacitor has not been reported to date.

Herein, an elastic and wearable ring-type supercapacitor (RTSC, Fig. 1) has been created to demonstrate high

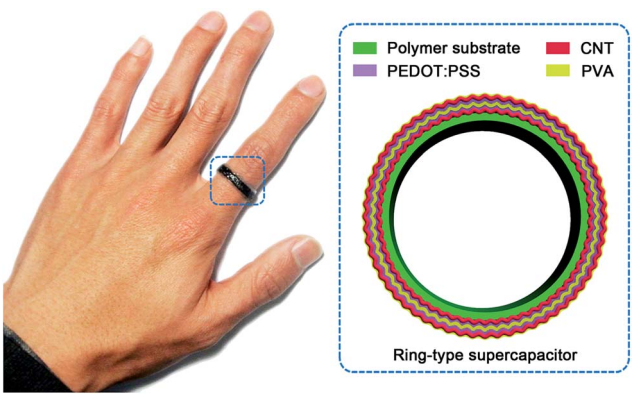

Fig. 1 Photograph (left image) and schematic illustration of the structure (right image) of the RTSC.

State Key Laboratory of Molecular Engineering of Polymers, Department of Macromolecular Science and Laboratory of Advanced Materials, Fudan University, Shanghai 200438, China. E-mail: zhanglijuan@fudan.edu.cn; penghs@fudan.edu.cn

† Electronic supplementary information (ESI) available. See DOI: 10.1039/c5ta10461k

electrochemical performances. This RTSC is fabricated by repeatedly winding aligned carbon nanotube (CNT) sheets and depositing poly(3,4-ethyl-enedioxythiophene):poly(styrene sulfonate) (PEDOT:PSS) onto an elastic ring substrate. The resulting device displays highly stable electrochemical properties under and after expanding and pressing. Therefore, it can be used with substrates of different sizes and shapes and may satisfy a variety of wearable applications as well as other fields.

Experimental section

Synthesis of the spinnable carbon nanotube array

The spinnable CNT array with a thickness of 220 μm was synthesized by chemical vapor deposition.[15] A silicon wafer deposited with Fe (1.2 nm)/Al_2O_3 (3 nm) was used as the catalyst. Ethylene (90 sccm) was used as the carbon source, and a gas mixture of argon (400 sccm) and hydrogen (30 sccm) was used as the carrier gas. The reaction was carried out at 740 °C for 10 min. The highly aligned CNT sheets were continuously drawn out of the spinnable CNT array.

Fabrication of the ring-type supercapacitor

An elastic ring substrate was obtained by injecting a precursor solution of Ecoflex 30 (Shanghai smarttech co., ltd, China) into a template, followed by curing at 80 °C for 2 h. The aligned CNT sheet was directly drawn from a spinnable CNT array and was attached onto the pre-expanded elastic ring substrate. The CNT sheet was carefully wrapped by continuously rotating the polymer ring. A thin layer of PEDOT:PSS (Clevios PH1000, mixed with 5% dimethylsulfoxide and 1% Zonyl FS-300 fluorosurfactant) was then coated onto the CNT sheet. Here the fluorosurfactant was used to promote wetting of the PEDOT:PSS in the aligned CNT. A polyvinyl alcohol (PVA)–H_3PO_4 gel electrolyte was prepared by mixing PVA powders (1 g) and H_3PO_4 (1.5 g) in deionized water (9 g). The gel electrolyte was coated onto the aligned CNT/PEDOT:PSS composite sheet and treated in a vacuum for 10 min at 40 °C. The second similar CNT/PEDOT:PSS composite sheet was wrapped, followed by coating the PVA gel electrolyte again. For convenience in characterization, the two electrodes were connected to the outer circuit by aligned CNT fibers that were prepared from the aligned CNT sheets (Fig. S1).† All the supercapacitors were characterized without further sealing.

Characterization

The structures were characterized by scanning electron microscopy (SEM, Hitachi, FE-SEM S-4800 operated at 1 kV). Galvanostatic charge–discharge curves and cyclic voltammograms of the RTSC were recorded on a CHI 660D electrochemical workstation. The long-term cyclic measurements were made at an Arbin electrochemical station (MSTAT-5 V/10 mA/16 Ch). The specific capacitance (C) of the RTSC was calculated from the equation of $C = 2I \times t/(M \times U)$, where I, t, M, and U correspond to the discharge current, discharge time, electrode weight and potential window, respectively. The gravimetric energy density (W) and gravimetric power density (P) were calculated from the equations of $W = 0.125 \times C \times U^2$ and $P = 3600 \times E/t$. The strain measurements were carried out by wrapping the RTSC onto cylinder-shaped substrates with different diameters.

Results and discussion

The structure and fabrication of the RTSC are schematically shown in Fig. 1 and S2.† An elastic ring electrode was first prepared by wrapping aligned CNT sheets onto an elastic polymer ring in a pre-expanded state (Fig. S3†). The aligned structure of the CNTs in the sheet originated from the array (Fig. S4 and S5†). Here the CNT exhibits a multi-walled structure with a diameter of ~10 nm and a length of ~220 μm.[16] A thin layer of PEDOT:PSS was then coated onto the CNT sheet to further increase the conductivity and capacitive performance, and this composite sheet served as the inner electrode. A layer of the PVA–H_3PO_4 gel electrolyte had been further coated onto the composite sheet. The second CNT/PEDOT:PSS composite sheet was next wrapped to function as the outer electrode, and the second layer of the gel electrolyte was finally coated to produce the RTSC after releasing to the relaxed state. The second electrolyte layer is used to not only improve the infiltration of the PVA electrolyte into active materials, but also prevent the outer electrode from being damaged.

Fig. 2a presents a typical SEM image of an aligned CNT sheet that is uniformly and stably attached onto the elastic polymer

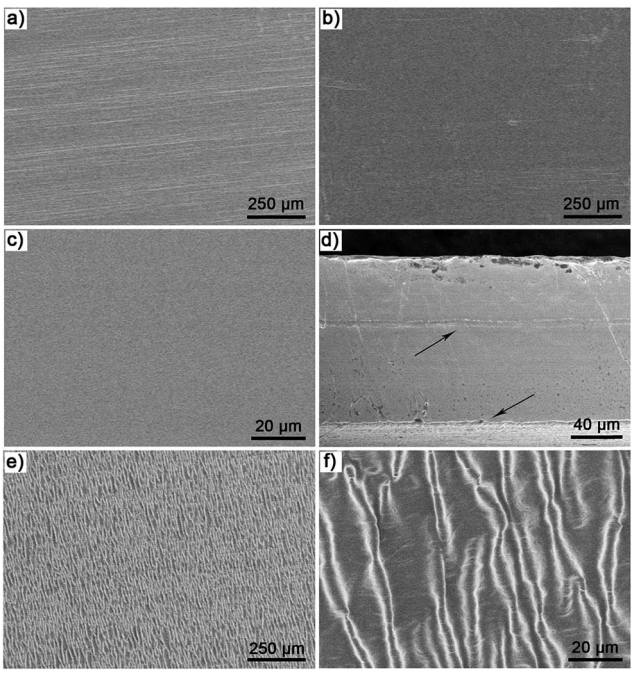

Fig. 2 SEM images of the RTSC. (a) Aligned CNT sheet on a stretched elastic polymer substrate. (b) PEDOT:PSS layer. (c) PVA gel electrolyte layer. (d) Cross-sectional image of the RTSC. The two arrows show the aligned CNT/PEDOT:PSS composite. (e and f) Rippled aligned CNT sheet on the released elastic polymer substrate at low and high magnifications, respectively.

substrate. An aligned CNT sheet from the spinnable array typically showed a thickness of ~18 nm,[16] and the thickness of the aligned CNT layer on the elastic polymer substrate can be increased by increasing the number of layers of wrapped CNT sheets (Fig. S3†). Fig. 2b shows a SEM image of the PEDOT:PSS layer, and the outer surface appears uniform without obvious aggregates, which is beneficial to improve the electrochemical performance of the RTSC. Similarly, the coated PVA gel electrolyte layer is also smooth and uniform (Fig. 2c). The cross-sectional SEM image further shows that the thickness of the gel electrolyte is ~75 μm and the two CNT/PEDOT:PSS composite sheets are separated by the electrolyte layer (Fig. 2d).

The aligned CNT sheets played a crucial role in achieving highly elastic and capacitive performance in the RTSC due to their high electrical conductivity and high flexibility. They typically exhibited electrical conductivities in the range of 10^2 to 10^3 S cm^{-1}.[17] The electrical resistance of the aligned CNT layer was decreased, *e.g.*, from 2.7 to 0.39 kΩ cm^{-1}, by increasing the thickness from 36 to 270 nm (Fig. S6†). The aligned CNTs formed a rippled structure after release to a relaxed state from the expanded substrate (Fig. 2e and f). The rippled structure facilitated the elasticity of the CNT sheet electrode with a high strain (*e.g.*, 100%) (Fig. S7†). The electrical resistance of the electrode was traced and it varied by less than 3% after repeatedly expanding and releasing for 1000 cycles at a strain of 100% (Fig. S8†), which was derived from the stable rippled structure under and after stretching (Fig. S9†).

The RTSCs based on aligned CNT layers with different thicknesses were first studied by galvanostatic charge–discharge measurements at a current density of 1 A g^{-1} (Fig. S10†). The specific capacitance was first increased from 14.5 to 32.1 F g^{-1} with increasing thickness from 36 to 180 nm due to the improved electrical conductivity of the CNT electrode; the specific capacitance was then reduced to 22.1 F g^{-1} with further increase to 270 nm as the gel electrolyte could not efficiently infiltrate into the inner CNT layer that was too thick. Therefore, the CNT layer with a thickness of 180 nm was studied below. To further enhance the capacitive performance, a series of conductive polymers such as polyaniline, polypyrrole and PEDOT:PSS can be used to improve the electrochemical performance.[18–20] As a demonstration, a thin layer of PEDOT:PSS was coated onto the aligned CNT sheet to prepare composite electrodes. Fig. S11† compares galvanostatic charge–discharge curves of the resulting RTSCs with different weight percentages of PEDOT:PSS. The specific capacitances had been largely increased after the incorporation of PEDOT:PSS because the highly conductive and oxygen-rich PEDOT:PSS enhanced both electrical and ionic conductivity.[20,21] A reversible redox reaction occurred during the charge-discharge process with electro-adsorption of protons

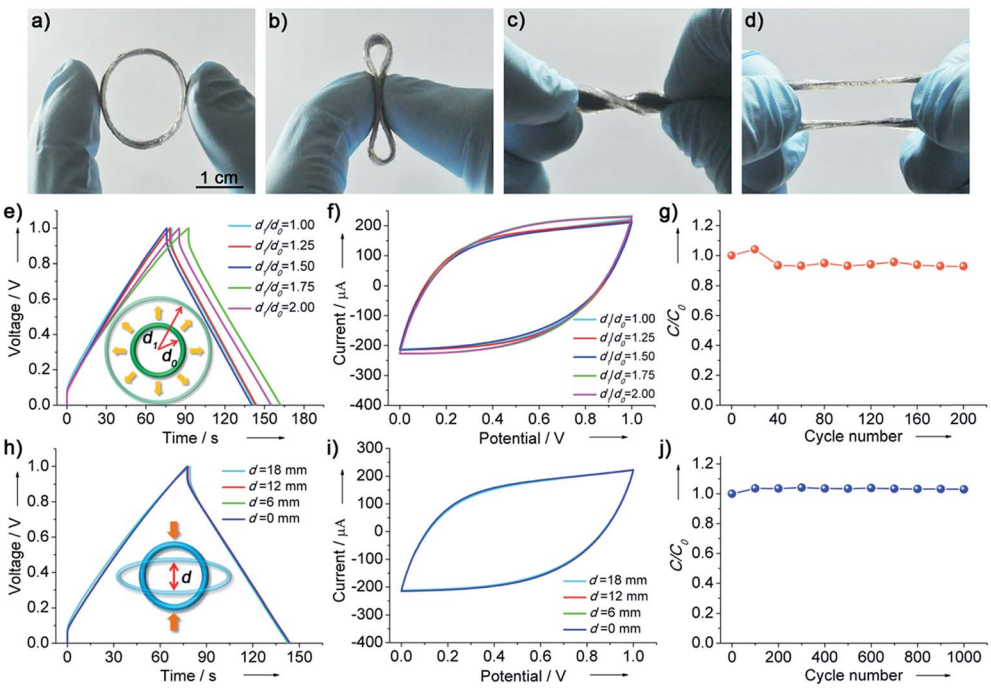

Fig. 3 Flexibility and elasticity of the RTSC. (a–d) Photographs of the RTSC being deformed into different shapes. (e and f) Galvanostatic charge–discharge curves and cyclic voltammograms of a RTSC before and after being expanded to 100% (*i.e.*, $d_1/d_0 = 2.00$), respectively. Here d_0 and d_1 correspond to the diameters of the RTSC before and after expanding, respectively. (g) Dependence of specific capacitance on the expanding cycle number at a strain of 75% (*i.e.*, $d_1/d_0 = 1.75$). C_0 and C correspond to the specific capacitances before and after expanding, respectively. (h and i) Galvanostatic charge–discharge curves and cyclic voltammograms of a RTSC before and after being pressed to different degrees, respectively. Here d is used to characterize the distance between the two pressed points. (j) Dependence of specific capacitance on the pressing cycle number with d of 0. C_0 and C correspond to the specific capacitances before and after pressing, respectively. The RTSC was fabricated from the CNT sheet with a thickness of 180 nm, and the PEDOT:PSS weight percentage was 65%. Charge/discharge current density: 1 A g^{-1}, scan rate: 50 mV s^{-1}.

and a fast electron transfer on the surface of the active material.[22] More specifically, the specific capacitance was increased from 32.1 to 85.0 and 134.8 F g^{-1} with increasing weight percentage from 0 to 35% and 65%; it decreased to 120.0 F g^{-1} at a higher weight percentage of 72%, which was mainly due to the difficulty in the infiltration of the gel electrolyte into dense active materials. The specific capacitance is further compared in Table S1,† and these RTSCs display a high electrochemical performance.[21,23–27] The maximal specific capacitance corresponds to a gravimetric energy density of 4.7 W h kg^{-1} and a gravimetric power density of 250 W kg^{-1}. The peak specific capacitance occurred at a weight percentage of 65% that had been incorporated in the following studies.

Fig. S12† further compares cyclic voltammograms of the RTSC at increasing scan rates from 20 to 200 mV s^{-1}. They shared a nearly rectangular shape at 20 and 50 mV s^{-1}, which indicated a high electrochemical stability. However, the rectangular shape could not be maintained at scan rates of 100 mV s^{-1} or above. This phenomenon may be explained by the fact that the concentration gradient at the electrode/electrolyte interface increases and the transient response falls off exponentially with increasing scan rate.[25] Fig. S13† shows the galvanostatic charge–discharge curves at increasing current densities from 0.5 to 4 A g^{-1}. The symmetry of the charge/discharge curves between 0 and 1 V signifies a high capacitive characteristic. To investigate the capacitance stability of the RTSC, a cyclic charging and discharging measurement was carried out at a current density of 1 A g^{-1} (Fig. S14†). It displayed capacity recession below 8% after over 2000 cycles.

The RTSC is flexible and can be deformed into a variety of shapes without an obvious decrease in the structural integrity (Fig. 3a–d). The high stability was further verified by tracing the electrochemical properties during expanding (Fig. 3e and f). The shapes of galvanostatic charge–discharge curves and cyclic voltammograms remained almost unchanged under expanding with increasing strain to 100%. Fig. S15† shows the specific capacitances with increasing strains, and they are increased from 134.8 to 149.1 F g^{-1} with the strain increasing from 0 to 100% (*i.e.*, d_1/d_0 = 1.00 to 2.00) due to the strain-induced enhancement in the contact between the gel electrolyte and electrode. Here d_0 and d_1 are defined as the diameters of the RTSC before and after expanding, respectively. The long-term elasticity was also investigated by repeatedly expanding the RTSC at a strain of 75% (*i.e.*, d_1/d_0 = 1.75). As expected, the specific capacitance was maintained at 92.9% after expanding for 200 cycles (Fig. 3g). In addition, the galvanostatic charge–discharge curves and cyclic voltammograms were traced under pressing with increasing strains (Fig. 3h and i). Similarly, the shapes of both galvanostatic charge–discharge curves and cyclic voltammograms were maintained with increasing strain, and the specific capacitances remained almost unchanged (Fig. S16†). Fig. 3j shows the dependence of specific capacitance on the pressing cycle number in the case that the top and bottom contact under pressing (*i.e.*, d = 0, and d is defined as

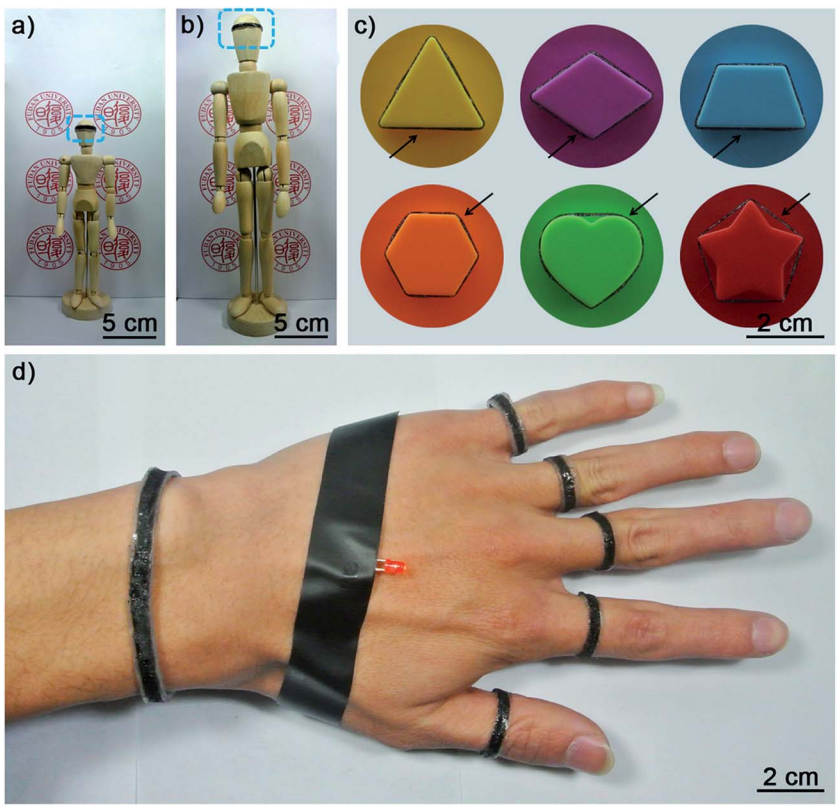

Fig. 4 (a and b) Photographs showing that the same RTSC was worn on the head of small and big puppets, respectively. (c) Photographs showing that the same RTSC was worn on a variety of shapes. (d) Photograph of six RTSCs being worn on a hand and fingers to power a red light emitting diode at the back of the hand.

the distance between the two pressing points at the top and bottom side). The specific capacitance was slightly increased by 3.6% in the first few cycles as the infiltration of the electrolyte had been improved for a better contact with the electrode under pressing and then remained stable even after 1000 cycles. Note that although the RTSC can also be achieved by connecting the two ends of a planer supercapacitor, the stretchability could be remarkably reduced owing to the low mechanical strength at the connecting point.

Due to the flexibility and elasticity, the same RTSC could satisfy a variety of substrates of different sizes (Fig. 4a and b) and shapes even with irregular surfaces (Fig. 4c). Therefore, it is suitable for different people by using the same size of RTSC and is particularly promising for wearable applications. The RTSC can also be designed with a configuration including different sections that were connected in series along the ring to tune the power capabilities for practical applications (Fig. S17†). For instance, the galvanostatic voltage window was doubled or tripled when two or three sections had been designed, respectively (Fig. S18†). The RTSC diameter can be also increased to satisfy different application requirements. For the diameter range in the wearable field, the specific capacitance of the RTSC remains almost unchanged with increasing size. In addition, six RTSCs can be worn onto hands and fingers to power light emitting diodes (Fig. 4d), which offers a new and promising strategy for future applications.

Conclusion

In summary, a new family of wearable RTSCs has been developed by winding aligned CNT/polymer composite sheets onto a ring substrate. The RTSC not only exhibits a high specific capacitance of 134.8 F g^{-1} but also shows high flexibility and elasticity, *e.g.*, the electrochemical performances are well maintained under expanding and pressing. They can effectively meet the requirements of a broad spectrum of substrates with different sizes and different shapes (even irregular shapes) in wearable and other flexible electronic devices. For practical applications in the future, we expect that an improved construction (*e.g.*, asymmetric supercapacitor), increased mass of active materials, and rigorous optimization would improve the device to drive more functional wearable devices.[28,29] Besides, the optimization of sealing technology, *e.g.*, three-dimensional packaging technology, is also needed for high stability and safety.[30] This strategy represents a general and efficient route to fabricate high-performance energy devices and can be also extended to the other power systems such as lithium ion batteries and solar cells.[31–33]

Acknowledgements

This work was supported by the NSFC (21225417, 51573027, 51403038, and 21471034), STCSM (15JC1490200, 12nm0503200, and 15XD1500400) and the Program for Outstanding Young Scholars from the Organization Department of the CPC Central Committee.

References

1 X. Wang, X. Lu, B. Liu, D. Chen, Y. Tong and G. Shen, *Adv. Mater.*, 2014, **26**, 4763.
2 F. X. Ma, H. Hu, H. B. Wu, C. Y. Xu, Z. C. Xu, L. Zhen and X. W. Lou, *Adv. Mater.*, 2015, **27**, 4097.
3 S. Zeng, H. Chen, F. Cai, Y. Kang, M. Chen and Q. Li, *J. Mater. Chem. A*, 2015, **3**, 23864.
4 Y. Hou, L. Chen, P. Liu, J. Kang, T. Fujita and M. Chen, *J. Mater. Chem. A*, 2014, **2**, 10910.
5 L. Qu, Y. Zhao, A. M. Khan, C. Han, K. M. Hercule, M. Yan, X. Liu, W. Chen, D. Wang, Z. Cai, W. Xu, K. Zhao, X. Zheng and L. Mai, *Nano Lett.*, 2015, **15**, 2037.
6 C. Zhu, P. Yang, D. Chao, X. Wang, X. Zhang, S. Chen, B. K. Tay, H. Huang, H. Zhang, W. Mai and H. Fan, *Adv. Mater.*, 2015, **27**, 4566.
7 J. Feng, S. Ye, A. Wang, X. Lu, Y. Tong and G. Li, *Adv. Funct. Mater.*, 2014, **24**, 7093.
8 X. Cao, B. Zheng, W. Shi, J. Yang, Z. Fan, Z. Luo, X. Rui, B. Chen, Q. Yan and H. Zhang, *Adv. Mater.*, 2015, **27**, 4695.
9 G. Ma, Z. Wang, B. Gao, T. Ding, Q. Zhong, X. Peng, J. Su, B. Hu, L. Yuan, P. K. Chu, J. Zhou and K. Huo, *J. Mater. Chem. A*, 2015, **3**, 14617.
10 G. Nystrom, A. Marais, E. Karabulut, L. Wagberg, Y. Cui and M. M. Hamedi, *Nat. Commun.*, 2015, **6**, 7259.
11 Y. Meng, Y. Zhao, C. Hu, H. Cheng, Y. Hu, Z. Zhang, G. Shi and L. Qu, *Adv. Mater.*, 2013, **25**, 2326.
12 L. Kou, T. Huang, B. Zheng, Y. Han, X. Zhao, K. Gopalsamy, H. Sun and C. Gao, *Nat. Commun.*, 2013, **5**, 3754.
13 L. Jing, Y. Zhou, Z. Cheng and T. Huang, *Sensors*, 2012, **12**, 5775.
14 B. H. Yang and S. Rhee, *Robot. Auton. Syst.*, 2000, **30**, 273.
15 Z. Zhang, X. Chen, P. Chen, G. Guan, L. Qiu, H. Lin, Z. Yang, W. Bai, Y. Luo and H. Peng, *Adv. Mater.*, 2014, **26**, 466.
16 Z. Zhang, K. Guo, Y. Li, X. Li, G. Guan, H. Li, Y. Luo, F. Zhao, Q. Zhang, B. Wei, Q. Pei and H. Peng, *Nat. Photon.*, 2015, **9**, 233.
17 H. Peng, X. Sun, F. Cai, X. Chen, Y. Zhu, G. Liao, D. Chen, Q. Li, Y. Lu, Y. Zhu and Q. Jia, *Nat. Nanotechnol.*, 2009, **4**, 738.
18 Z. Tong, Y. Yang, J. Wang, J. Zhao, B. L. Su and Y. Li, *J. Mater. Chem. A*, 2014, **2**, 4642.
19 W. Xiong, X. Hu, X. Wu, Y. Zeng, B. Wang, G. He and Z. Zhu, *J. Mater. Chem. A*, 2015, **3**, 17209.
20 Z. Su, C. Yang, C. Xu, H. Wu, Z. Zhang, T. Liu, C. Zhang, Q. Yang, B. Li and F. Kang, *J. Mater. Chem. A*, 2013, **1**, 12432.
21 T. Chen, R. Hao, H. Peng and L. Dai, *Angew. Chem., Int. Ed.*, 2015, **54**, 618.
22 P. Simon and Y. Gogotsi, *Nat. Mater.*, 2008, **7**, 845.
23 Z. Yang, J. Deng, X. Chen, J. Ren and H. Peng, *Angew. Chem., Int. Ed.*, 2013, **52**, 13453.
24 Z. Zhang, J. Deng, X. Li, Z. Yang, S. He, X. Chen, G. Guan, J. Ren and H. Peng, *Adv. Mater.*, 2015, **27**, 356.
25 D. Antiohos, G. Folkes, P. Sherrell, S. Ashraf, G. G. Wallace, P. Aitchison, A. T. Harris, J. Chen and A. I. Minett, *J. Mater. Chem.*, 2011, **21**, 15987.

26 G. P. Pandey, A. C. Rastogi and C. R. Westgate, *J. Power Sources*, 2014, **245**, 857.
27 Z. Niu, H. Dong, B. Zhu, J. Li, H. H. Hng, W. Zhou, X. Chen and S. Xie, *Adv. Mater.*, 2013, **25**, 1058.
28 Y. Fu, X. Cai, H. Wu, Z. Lv, S. Hou, M. Peng, X. Yu and D. Zou, *Adv. Mater.*, 2012, **24**, 5713.
29 Y. Fu, H. Wu, S. Ye, X. Cai, X. Yu, S. Hou, H. Kafafy and D. Zou, *Energy Environ. Sci.*, 2013, **6**, 805.
30 K. N. Tu, *Microelectron. Reliab.*, 2011, **51**, 517.
31 I. Y. Jeon, M. J. Ju, J. Xu, H. J. Choi, J. M. Seo, M. J. Kim, I. T. Choi, H. M. Kim, J. C. Kim, J. J. Lee, H. K. Liu, H. K. Kim, S. Dou, L. Dai and J. B. Baek, *Adv. Funct. Mater.*, 2015, **25**, 1170.
32 Q. Zhang, B. Kan, X. Wan, H. Zhang, F. Liu, M. Li, X. Yang, Y. Wang, W. Ni, T. P. Russell, Y. Shen and Y. Chen, *J. Mater. Chem. A*, 2015, **3**, 22274.
33 X. Fan, Z. Chu, F. Wang, C. Zhang, L. Chen, Y. Tang and D. Zou, *Adv. Mater.*, 2008, **20**, 592.